crystals

MDPI

Article

The Effect of Martensitic Phase Transformation Dilation on Microstructure, Strain–Stress and Mechanical Properties for Welding of High-Strength Steel

Xizhang Chen [1,2,*], Pengfei Wang [1,3], Qiuhong Pan [3] and Sanbao Lin [2]

1 School of Mechanical and Electrical Engineering, Wenzhou University, Wenzhou 325035, China; wpfsmh@163.com
2 State Key Lab of Advanced Welding and Joining, Harbin Institute of Technology, Haerbin 150001, China; sblin@hit.edu.cn
3 School of Materials Science and Engineering, Jiangsu University, Zhenjiang 212013, China; panhong9004@163.com
* Correspondence: kernel.chen@gmail.com or chenxizhang@wzu.edu.cn

Received: 16 May 2018; Accepted: 2 July 2018; Published: 15 July 2018

Abstract: The application of low transformation temperature (LTT) wire can effectively reduce residual stress, without the need for preheating before welding and heat treatment after welding. The mechanism reduces the martensitic transformation temperature, allowing the martensite volume expansion to offset some or all of the heat-shrinking, resulting in reduced residual stress during the welding process. In this paper, commercial ER110S-G welding wire and LTT wire with chemical composition Cr10Ni8MnMoCuTiVB were developed to solve the problem of stress concentration. The microstructure of the LTT joint is mainly composed of martensite and a small amount of residual austenite, while the microstructure of the ER110S-G joint is mainly composed of ferrite and a small amount of granular bainite. The micro-hardness and tensile strength of the LTT joint is higher than that of ER110S-G joint; however, the impact toughness of the LTT joint is not as good as that of the ER110S-G joint. The martensitic phase transformation of LTT starts at 212 °C and finishes at around 50 °C, and the expansion caused by phase transition is about 0.48%, which is much higher than that of the base metal (0.15%) and ER110S-G (0.18%). The residual tensile stress at the weld zone of the ER110S-G joint is 175.5 MPa, while the residual compressive stress at the weld zone of LTT joint is −257.6 MPa.

Keywords: martensite; phase transformation; microstructure; mechanical properties; residual stress

1. Introduction

With the characteristics of high strength and excellent weldability, high-strength low-alloy steel is widely used in automobiles, railway vehicles, bridges and other industries [1,2]. In the process of welding steel, it is easy to generate large and centralized residual stresses, which may produce stress corrosion cracking and brittle fracture, seriously reduce the anti-fatigue performance, and greatly reduce the service life of the components [3–6]. The mechanical and heat treatment methods are usually used to reduce or eliminate the welding residual stress. Obviously, these additional measures inevitably lead to an increase in costs. The application of low transformation temperature (LTT) wire can effectively reduce the residual stress, without the need for preheating before welding and heat treatment after welding [7,8]. The mechanism reduces the martensitic transformation temperature, allowing the martensite volume expansion to offset some or all of the heat-shrinking, resulting in

reduced tensile residual stress during welding process. This not only reduces the production cost, but also improves the fatigue resistance of the welded components [9].

Dai et al. [10] used the traditional commercial OK75.78 wire and the low transformation temperature (LTT) wire to weld two comparable Weldox960 base plates. The residual stress of the joints were measured using neutron diffraction, with the results showing that LTT can effectively reduce the welding residual stress of high-strength steel welding and improve the stress distribution. Chiaki and Shiga [11] found that the residual stress distribution is ideal when the starting temperature of martensite transformation is 200 °C, and the residual compressive stress at the weld toe is 300 MPa.

Ohta et al. [12] found that by using the 10 Cr–10 Ni–0.7 Mn wire the fatigue limit of the LTT joint could be twice that of conventional joints. Barsoum et al. [13] studied the effect of residual stress on fatigue strength. Fatigue tests showed that the LTT joint had a 40% increase in fatigue strength compared to conventional joints. Fabrice et al. [14] found that the LTT wire significantly improved the fatigue strength of the joint, and the fatigue strength was 60% higher than that of the conventional wire (G3Si1) filling joint in two million cycles. Wang et al. [15] compared the conventional wire of C–Mn and LTT wire of 9.1 Cr–8.5 Ni–1.25 Mn, and showed that the fatigue strength was improved by 59% when using LTT wire. Altenkirch et al. [16] simulated the stress state of the welded structure during service and analyzed the changes in its organization and performance. The results showed that the low transformation temperature material can effectively reduce the effect of the external load and thus improve the ability of the welded structure to resist the external load.

Miki et al. used LTT wire to repair a fatigue breakage and found that the LTT wire could prevent crack initiation and expansion, thereby increasing the fatigue strength of the joints [17]. Zenitani et al. [18] found that the metal welded by LTT wire with a phase-transition temperature of 94 °C consisted of most of the martensite and a small amount of retained austenite (RA), with a good performance of crack resistance and the ability to potentially avoid cold cracks. Y. Mikami et al. [19–22] found that the angular deformation of welded joints using LTT wire was significantly smaller than that of traditional wire. Shirzadi et al. [23] also studied the influence of LTT materials on welding deformation. The experimental results showed that the welding residual deformation can be effectively relieved when LTT wire is used. The research of low temperature phase materials has achieved certain results. However, the temperature field and formation of residual stress within thick and thin plates are totally different. In order to explain the formation mechanism of residual stress in thick plates, more research and experiments are needed.

In this paper, one kind of low transformation temperature (LTT) wire was developed to solve the problem of stress concentration of high-strength low-alloy steels during welding. Quenched and tempered high-strength steel Q690D was selected as the base plate material, and was welded with self-developed LTT wire and the traditional commercial wire ER110S-G for comparison. The microstructure, mechanical properties and welding residual stress were then evaluated and compared.

2. Experimental Procedure

In the experiment, a direct-reading spectrometer (SPECTRO MAXx mm06, SPECTRO, Kleve, Germany) and metallographic microscope (ZEISS, Oberkochen, Germany) were used to measure the composition and microstructure of welding materials. The welding base material is low-alloy high-strength steel Q690D. The chemical composition and mechanical properties are shown in Table 1. The supply state of Q690D is quenched and tempered, and the matrix is tempered bainite, as shown in Figure 1.

Table 1. The chemical composition and mechanical properties of quenched and tempered Q690D.

Component	C	Si	M_n	P	S	Ni	Cr	Mo	Nb	Ti	V	Fe
Wt (%)	0.11	0.31	1.27	0.009	0.002	0.03	0.23	0.01	0.012	0.023	0.03	Bal.
Mechanical property	Yield strength Rp0.2 (MPa)			Tensile strenth Rm (MPa)		Elongation(%)			Impact absorbing energy of −20 °C (J)			
	>690			810		17			220			

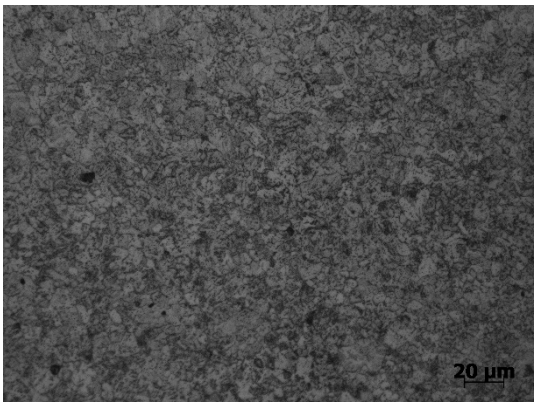

Figure 1. The microstructure of Q690D.

One kind of low transformation temperature (LTT) wire was designed. Its alloy composition is as shown in Table 2. A conventional welding wire (ER110S-G) with a 1.2 mm diameter is used to make a contrast test against LTT wire. The chemical composition and mechanical properties are shown in Table 3.

Table 2. Composition of designed LTT wire (wt. %).

Component Wt (%)	C	Ni	Cr	Si	Mn	Mo	Cu	Ti	V	B	Nb	CE	Fe
LTT	0.06	8	10	0.3	0.6	0.5	0.5	0.2	0.25	0.002	0.01	0.1	Bal.

Cr10Ni8MnMoCuTiVB.

Table 3. The chemical composition and mechanical properties of ER110S-G.

Component	C	Si	Mn	P	S	Ni	Cr	Mo	Fe
Wt (%)	0.094	0.53	1.62	0.013	0.01	1.57	0.29	0.34	Bal.
Mechanical property	Yield strength Rp0.2 (MPa)			Tensile strength Rm (MPa)		Elongation(%)		Impact absorbing energy of −20 °C (J)	
	740			820		17		80	

The experiment uses metal active gas welding (MAG) and the sample size is 300 × 120 × 10 mm, as shown in Figure 2. The weld groove has an angle of 60 ° and the root gap is 2 mm, as shown in Figure 3. Using three-layers of welding, the process parameters are as shown in Table 4.

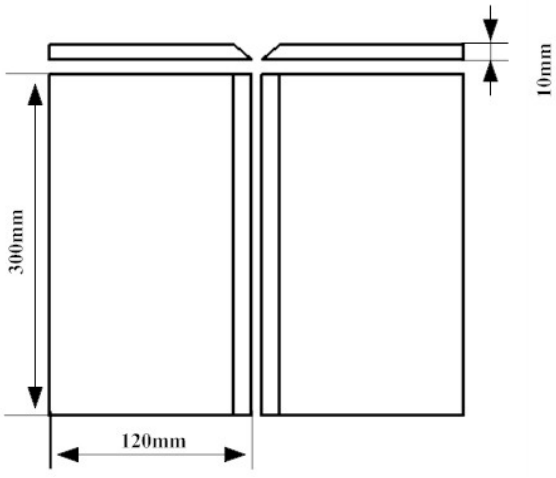

Figure 2. Weld geometry.

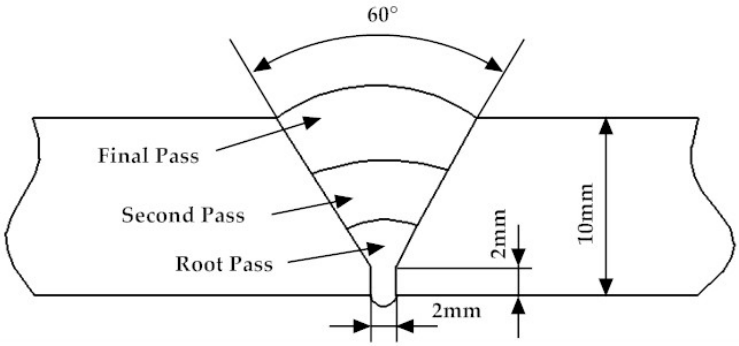

Figure 3. Joint groove.

Table 4. The welding parameters.

Subject	Root Pass	Second Pass	Final Pass
Welding current	133 A	200 A	209 A
Welding voltage	21.0 V	23.8 V	24.1 V
Wire feed speed	4.2 m/min	7.0 m/min	7.2 m/min
Travel speed	6 mm/s	5 mm/s	4 mm/s
Shielding gas	80% Ar + 20% CO_2	80% Ar + 20% CO_2	80% Ar + 20% CO_2
Gas flow	15 L/min	15 L/min	15 L/min

The LTT joint metallographic sample corrosion liquid ratio is 10 g $FeCl_3$ + 30 mL HCl + 120 mL H_2O, while the ER110S-G joint metallographic specimens used 4% nitric acid alcohol corrosion. The microstructures of the specimens were observed by optical microscope (OM) and scanning electron microscope (SEM). The phase-transition temperature was measured by Gleeble3500 thermal simulator (Dynamic Systems Inc., New York, NY, USA). The residual stress of the joint was measured by X-ray diffraction. In addition, the microhardness, impact toughness and tensile strength of the joint were tested to analyze the properties of the joint.

3. Results and Discussions

3.1. Microstructure

The microstructure of joints were observed by Leica MEF-4M optical microscope (Leica Company, Barnack, Germany). It can be seen from Figure 4a that the microstructure of the weld zone of the LTT joint is mainly composed of martensite and a small amount of retained austenite (RA). The martensite structure is composed of a large number of lath martensite (LM) and a small number of acicular martensite (AM). Compared with Figure 4c,d, the amount of retained austenite (RA) in the root layer is lower than that of the final layer. The main reason for this is that the heat source of the cover layer will have a tempering role to the backing layer, which will lead to transformation of the retained austenite (RA).

As shown in Figure 4b, the microstructure of the weld zone in the ER110S-G joint is mainly composed of tiny acicular ferrite and a small amount of granular bainite. As shown in Figure 4e,f, the fusion zone is relatively narrow. The boundary parent metal provides the nucleation site for the liquid metal, many sub crystals are formed, and the new dendrites grow into the weld center with the subgrain as a matrix. The grain size of the fusion zone is different, and is mainly composed of the granular bainite (GB) structure and the lath bainite (LB) structure. Figure 4g,h are the heat-affected zone of LTT and ER110S-G joints, mainly consisting of lath martensite and bainite. The grains are coarse, the main reason for which is heating during the welding thermal cycle leading to the formation and growth of grains.

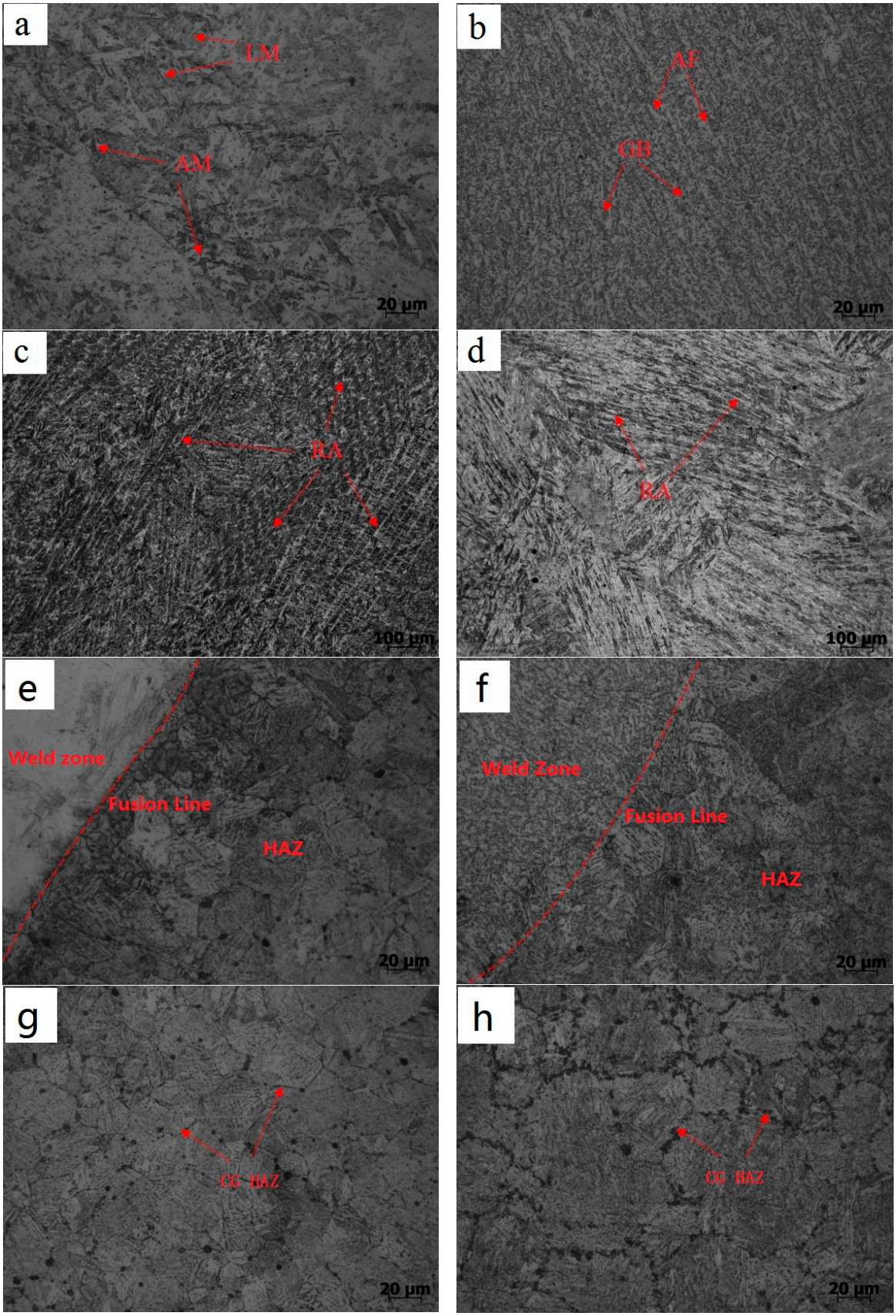

Figure 4. Microstructure of welded joints :(**a**) welding seam of LTT; (**b**) welding seam of ER110S-G; (**c**) the third layer of LTT; (**d**) the first layer of LTT; (**e**) fusion zone of LTT; (**f**) fusion zone of ER110S-G; (**g**) Coarse grain zone of LTT; (**h**) Coarse grain zone of ER110S-G.

In this experiment, the microstructure and element distribution of welded joints were analyzed by JEOL-JSM-7001F type thermal field-emission scanning electron microscopy (JEOL Ltd., Tokyo, Japan) and energy-dispersive spectrometry, respectively. The resolution ratio of thermal field-emission scanning electron microscopy was 1.2 nm (30 kV)/3.0 nm (1 kV) and the magnification of it adopted 10–800 K. As shown in Figure 5a, the microstructure of the weld zone in the LTT joint is composed of a large number of lath martensite and some acicular martensite. From Figure 5c, it can be seen that there is a small amount of residual austenite between the lath martensite. Figure 5d is the fusion zone of the LTT joint, showing that the weld organization is relatively small, and the microstructure of the heat-affected zone is coarse. From Figure 5b, the microstructure of the weld zone is composed of a large number of acicular ferrite and some granular bainite. It is observed that the grain size in Figure 5e is obviously larger than the grain size of Figure 4f. In addition, the grain distribution in the fine crystal region is even.

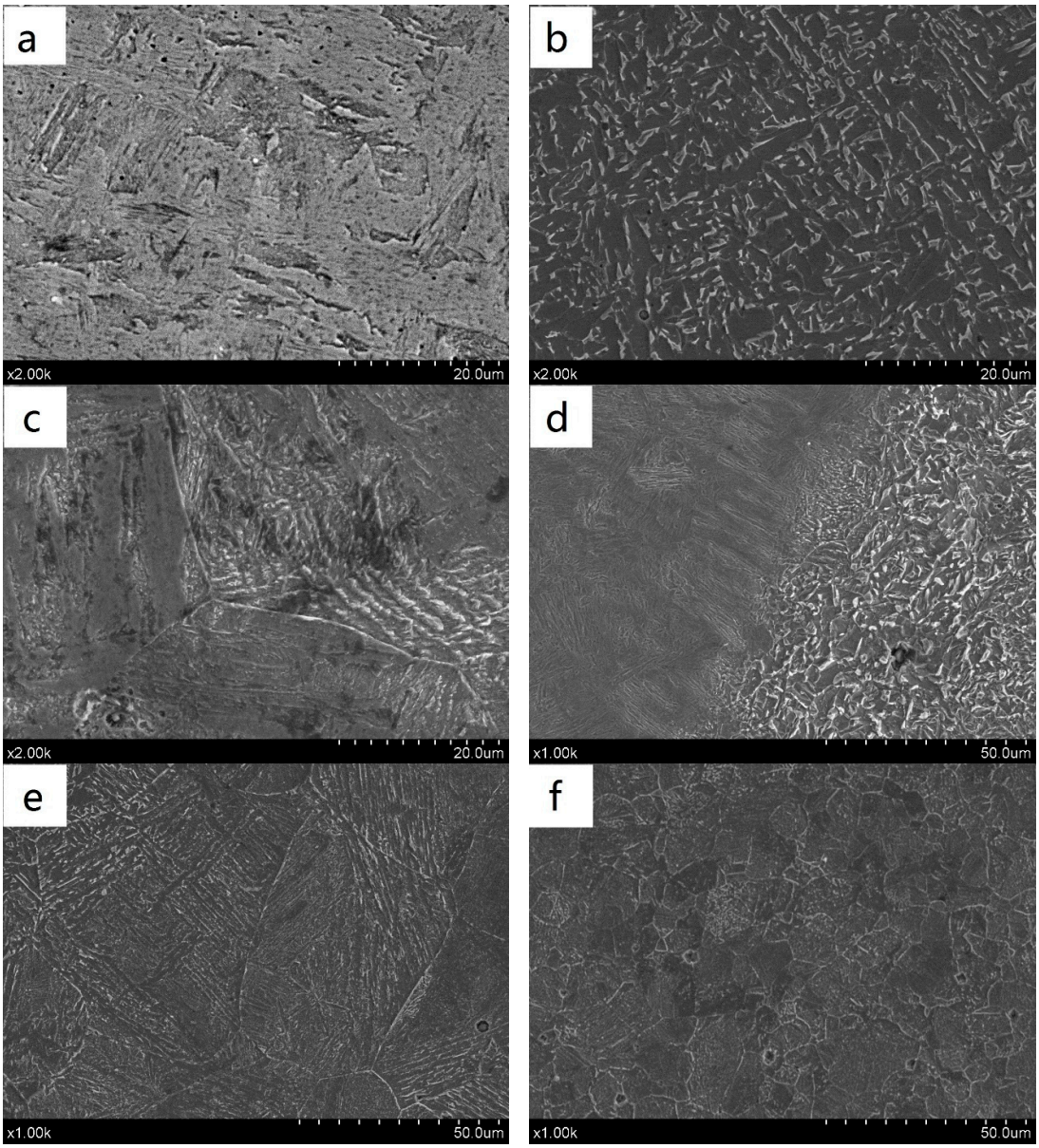

Figure 5. SEM morphology of welded joints :(**a**) welding seam of LTT; (**b**) welding seam of ER110S-G (**c**) retained austenite (RA) of LTT; (**d**) fusion zone of LTT; (**e**) Coarse grain zone of ER110S-G; (**f**) fine grain zone of ER110S-G.

Figure 6a is the EDS analysis area in the weld zone of the LTT joint, with the joint's element composition shown in Table 5. Figure 6b is the EDS analysis area in the weld zone of the ER110S-G joint, with the joint's element composition shown in Table 6. As shown in Figure 6c, the concentration of Cr and Ni in the weld zone of the LTT welding is obviously higher than that of Cr and Ni in the heat-affected zone, indicating that the diffusion of Cr and Ni elements occurred during the welding process. As shown in Figure 6d, the concentration of Cr, Ni, Mn, Si and other major alloy elements in the ER110S-G joint changes little on both sides. The main reason is that the composition of the ER110S-G welding wire is similar to that of the parent metal.

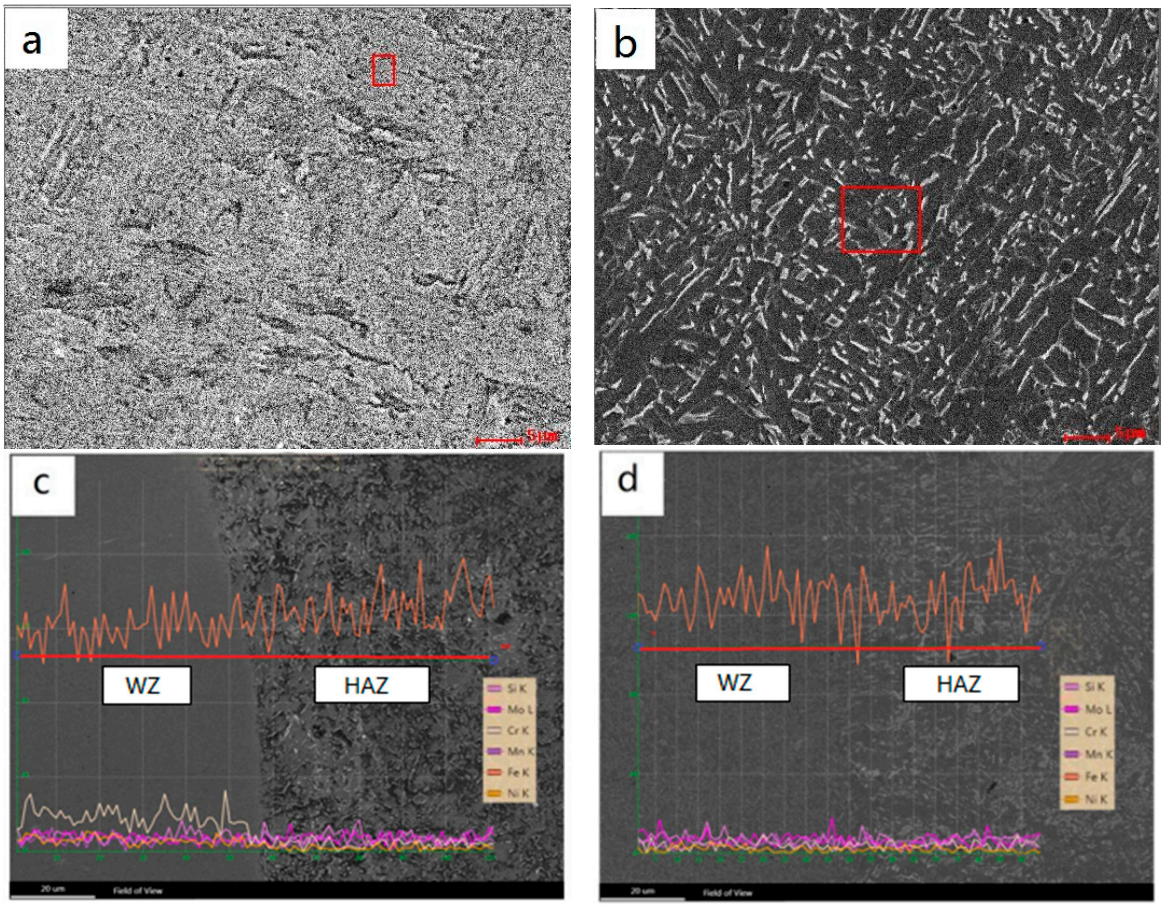

Figure 6. EDS analysis of the welds: (**a**) welding seam of LTT ;(**b**) welding seam of ER110S-G; (**c**) the line scanning of LTT ;(**d**) the line scanning of ER110S-G.

Table 5. Element composition of LTT joint.

Element	Wt %	At %
C	0.85	3.83
Fe	74.16	71.68
Cu	1.74	1.48
Ti	0.53	0.60
V	1.11	1.17
Cr	10.11	10.50
Mn	2.63	2.59
Ni	8.87	8.15
Total	100	100

Table 6. Chemical composition of ER110S-G joint.

Element	Wt %	At %
C	0.63	2.87
Cu	2.07	1.78
Ti	0.82	0.93
V	1.17	1.26
Cr	1.09	1.15
Mn	3.17	3.14
Fe	90.37	88.24
Ni	0.68	0.63
Total	100	100

3.2. Microhardness

It can be seen from Figure 7a that the microhardness of the weld zone of the LTT joint is significantly higher than that of the base metal (about 265 HV~275 HV). The main reason for this is that the microstructure of the weld zone is dominated by hard martensite, so the microhardness of the weld zone is much higher than that of the base metal, with the peak value of microhardness being up to 383 HV. As shown by Figure 7b, the microhardness of the weld zone of the ER110S-G joint is 255 HV, slightly lower than the hardness. The main reason for this is that the microstructure of the weld zone is composed of a large number of acicular ferrite and granular bainite, with good plasticity and toughness, but relatively low hardness.

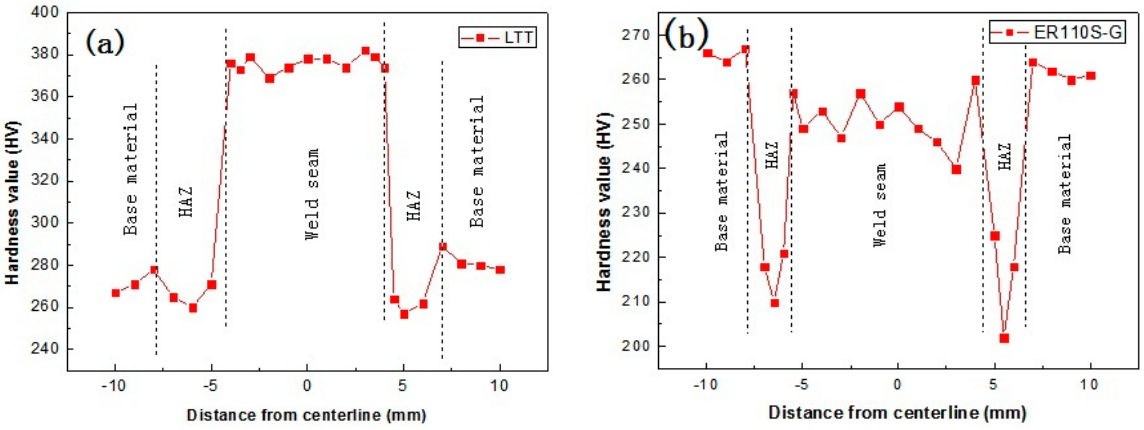

Figure 7. Micro-hardness of weld joints (**a**) LTT joint and (**b**) ER110S-G joint.

3.3. Impact

The joint impact test results are shown in Table 7. The impact absorbing energy of the weld zone of the ER110S-G joint is 105 J, while the impact absorbing energy of the weld zone of the LTT joint is only 36 J, far below that of the ER110S-G joint. The main reason is that the microstructure of the weld zone in ER110S-G is composed of a large number of ferrite and some granular bainite. The plasticity and toughness of ferrite are better, so the matrix exhibits good impact toughness. The microstructure of the LTT weld is mainly composed of martensite and a small amount of retained austenite (RA). Martensite has high strength and hardness, but its toughness is not enough, leading to its low impact absorption.

Figure 8a shows the impact fracture morphology of the LTT joint, demonstrating a brittle fracture. This shows river patterning, observed at the inclusions and pores, with a certain amount of tear ridges. The impact fracture of the ER110S-G weld zone is full of equiaxed dimples, and the dimple distribution is dense, small and deep. This contributes to the conclusion that the fracture mode of the ER110S-G joint is ductile, as shown in Figure 8b. The ER110S-G weld zone has high toughness,

with the main reason for this being that the ER110S-G joint weld organization is composed of a large number of acicular ferrite and granular bainite structures. The acicular ferrite is formed in the interior of the original austenitic grains, with a large angle dispersion. Thus, when the crack wants to transverse, it must constantly change its direction and path of expansion, thereby consuming more energy. Therefore, the ability of crack propagation can be improved, and the toughness of the weld zone is greatly improved, with the joints mainly fracturing in a ductile manner.

Table 7. Impact properties of weld joints.

Sample	Test Area	Impact Absorbing Energy (J)
LTT	WZ	36
	FZ	43
	HAZ	78
ER110S-G	WZ	105
	FZ	63
	HAZ	81

Figure 8c,d shows the impact fracture morphology of the fusion zone, demonstrating a brittle fracture. River and tongue patterns may be observed, with micro-cracks and less inclusions also being present. Figure 8e,f shows the impact fracture morphology of the heat-affected zone, demonstrating a mix of a brittle and ductile fracture. Here, the fracture morphology and fusion area looks similar, with a river pattern and a small amount of intragranular dimpling being visible.

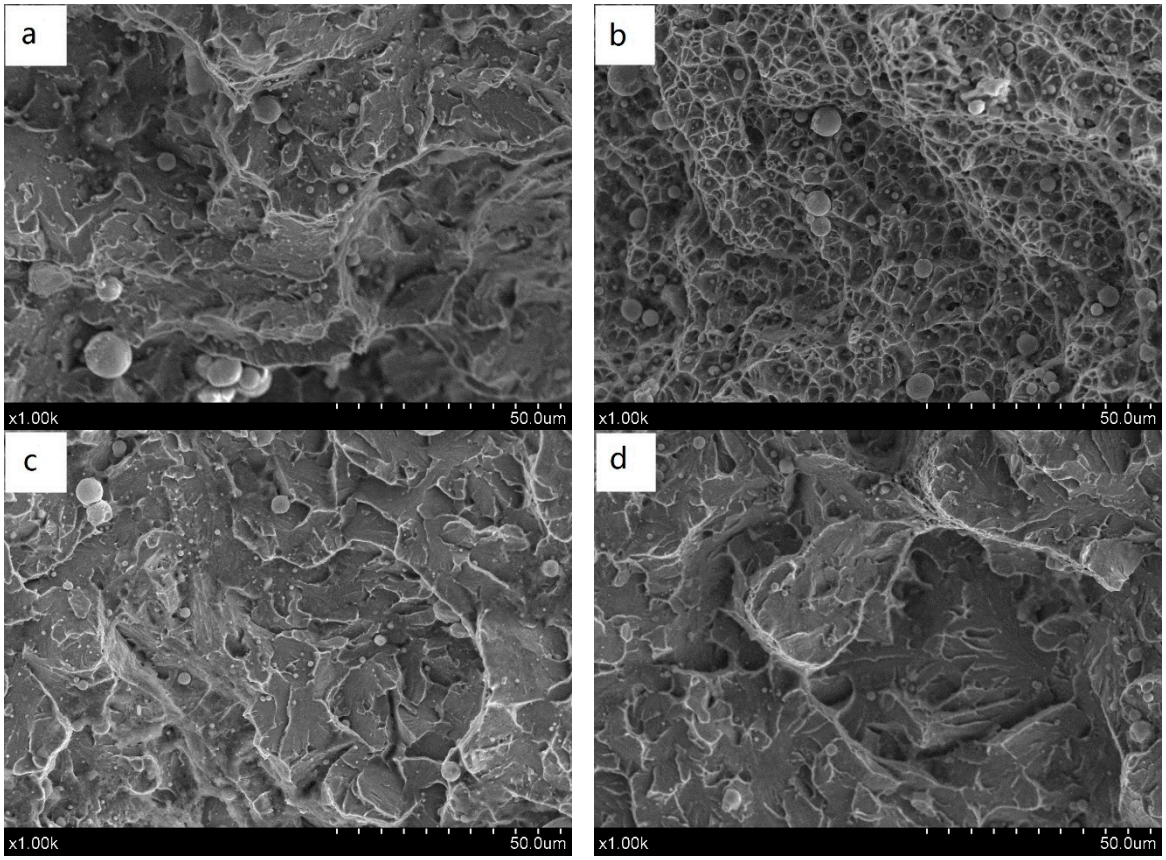

Figure 8. *Cont*.

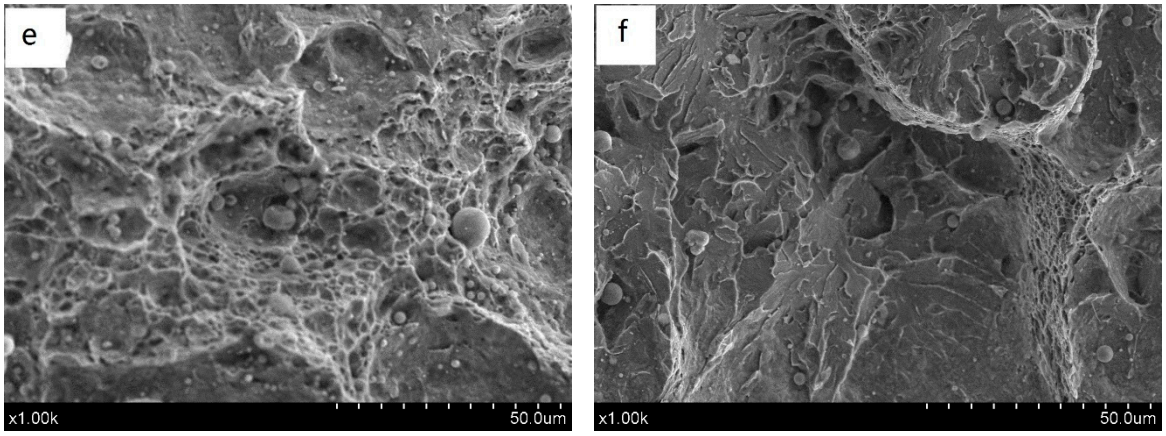

Figure 8. Impact fracture morphology of weld joints:(**a**) welding seam of LTT; (**b**) welding seam of ER110S-G; (**c**) fusion zone of LTT; (**d**) fusion zone of ER110S-G; (**e**) HAZ of LTT ;(**f**) HAZ of ER110S-G.

3.4. Tensile Properties

The tensile test results of the welds are shown in Table 8. The LTT tensile test specimens and ER110S-G tensile test specimens were broken in the heat-affected zone. The elongation rates of LTT and ER110S-G tensile specimens are 9.8% and 13.6%, respectively. The tensile strength of the joints is 797.3 MPa and 788 MPa, respectively.

Table 8. Tensile testing results of the welds.

Sample	Yield Strength Rp0.2 (MPa)	Average of Rp0.2 (MPa)	Tensile Strength Rm (MPa)	Average of Rm (MPa)	Elongation(%)	Fracture Location
LTT	722	727	793	797.3	9.8	HAZ
	731		801			HAZ
	727		798			HAZ
ER110S-G	723	722	789	788	13.6	HAZ
	718		781			HAZ
	726		794			HAZ
Q690D	≥690	-	810	-	17	BM

3.5. Phase Temperature

The specimen with a size of Φ 6 × 76 mm was intercepted from the weld joint and we tested for its phase-transition temperature on a Gleeble3500 thermal simulator. The sample was first heated to 900 °C at a rate of 10 °C/s, then subjected to austenitization for 5 min, and finally cooled to room temperature at a rate of 10 °C/s (with a thermal simulated heating curve as shown in Figure 9). As shown in Figure 10, it can be seen that the Q690D matrix material starts to change at about 440 °C and finishes at around 360 °C, with the phase change being about 0.15%. The starting temperature of phase-transition for the ER110S-G sample is about 600 °C, and finishes at around 460 °C, with the phase change expansion rate being 0.18%. Finally, the starting temperature for the martensitic transformation of the LTT sample is about 212 °C, and finishes at around 50 °C, with the phase change expansion rate being 0.48%.

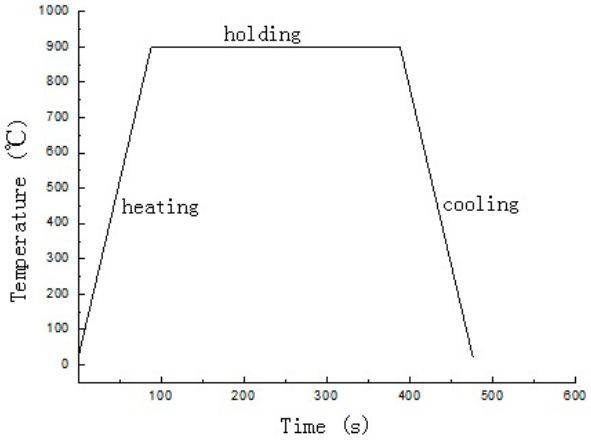

Figure 9. The schematic of thermal simulation cycling curve.

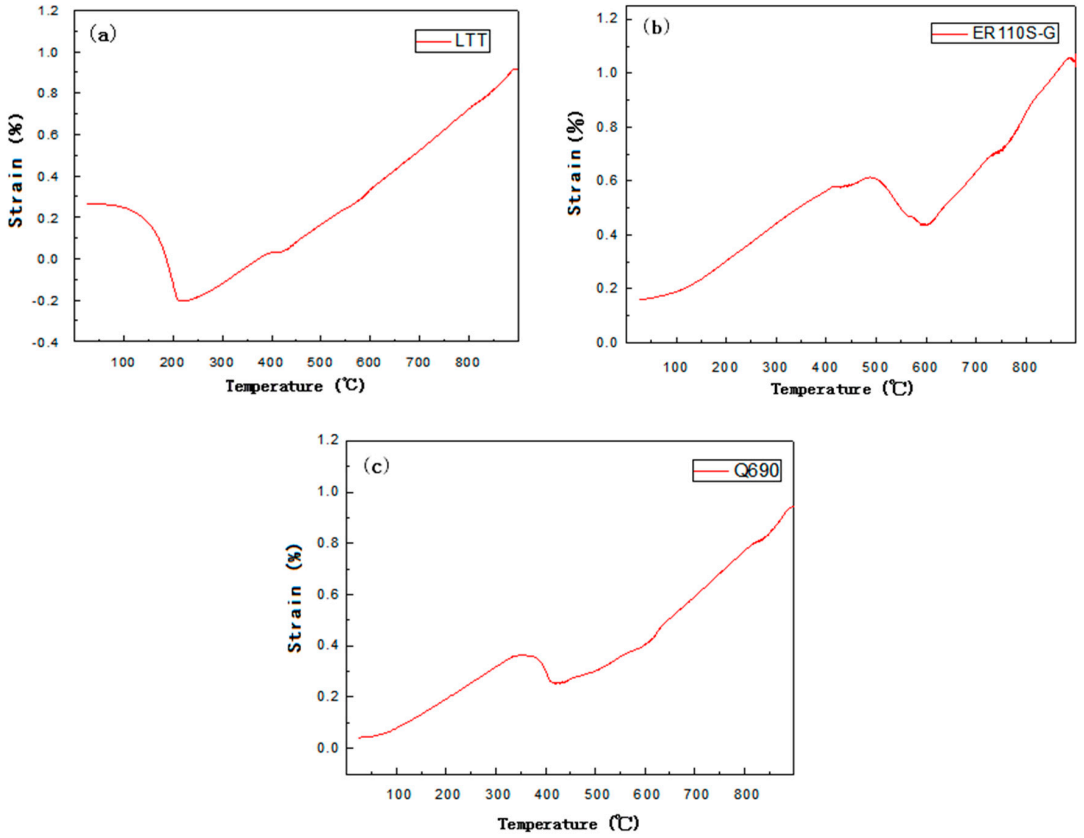

Figure 10. Strain curves with temperature of different weld metals (**a**) LTT weld, (**b**) ER110S-G weld, and (**c**) base metal Q690.

3.6. Residual Stress

The welding residual stress test points are distributed perpendicular to the weld, and the distances from the weld centerline are 0, 3, 10, 15, 20, 25, 30, 40, 50, 6, 60, 70, and 80 mm, as shown in Figure 11. The welding residual stress distribution is shown in Figure 12, with the residual tensile stress value for the ER110S-G joint being about 175.5 MPa. Initially, an increase of distance from the center of the weld results in an increase in residual tensile stress, until a maximum is reached and the residual tensile stress decreases to 0 MPa. The residual tensile stress reaches the maximum value of about 468.7 MPa in the heat-affected zone. The residual compressive stress at the center of the LTT joint welds

is −257.6 MPa. The cause of welding residual stress in low transformation temperature phase-change materials is the martensitic transformation, which occurs in the lower temperature region of the welding cooling process. In the weld, this transformation is generated by an expansion and contraction which exceeds that of the welding cooling process. In the weld area, the expansion, extrusion and interaction of the adjacent parent material is constrained within the heat-affected zone. At 6mm away from the weld center line, the welding residual stress for the LTT joint is only 295.7 MPa, far less than that of the ER110S-G joint. The results show that the LTT phase-change material tested here can reduce the residual tensile strength of joints.

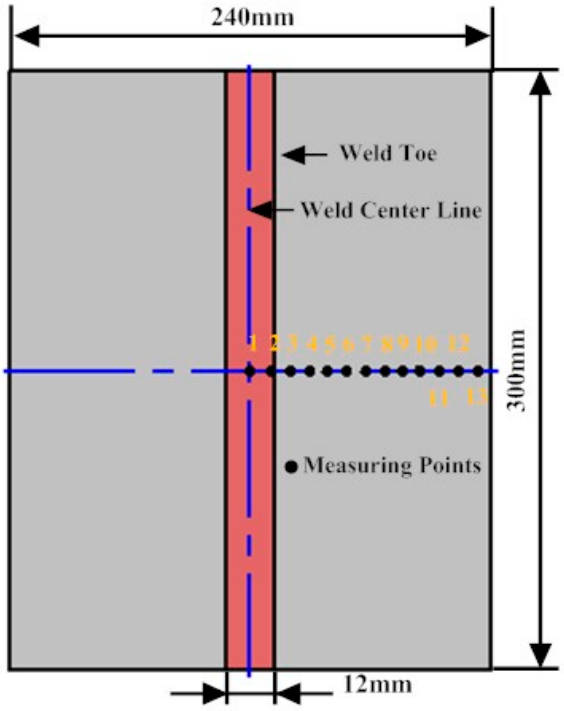

Figure 11. The measuring points of residual stress.

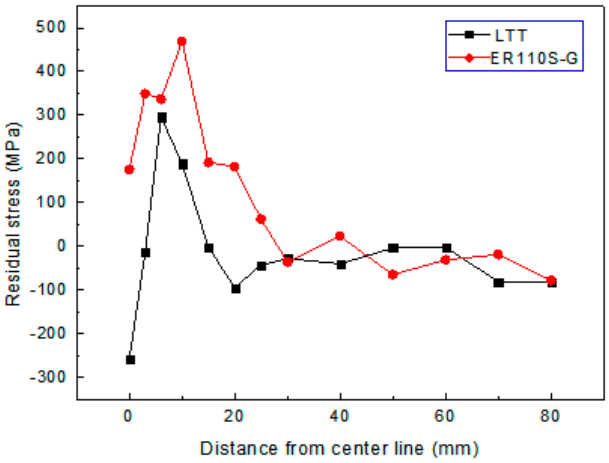

Figure 12. The residual stresses distribution of weld joints.

3.7. Welding Deformation Analysis

The welding residual stress is closely related to the formation of welding deformation. During the welding process, the component will produce complex internal stresses, which will lead to the

deformation of the weldment. Figure 13 shows the weld deformation of the (a) LTT joint and the (b) ER110S-G joint. The degree of welding deformation can be measured according to the following model (as shown in Figure 14). First, the shrinkage of the welding test plate in the length direction is neglected, and then the angular deformation radian of the welding test plate can be calculated according to the following equation:

$$\delta = \delta_1 + \delta_2 = \frac{d_1 + d_2}{L} \tag{1}$$

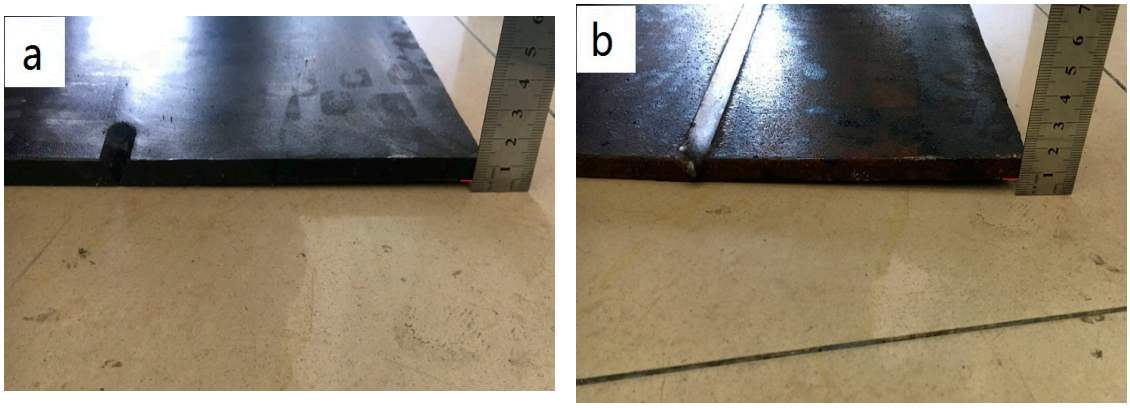

Figure 13. Welding deformation of (**a**) LTT and (**b**) ER110S-G weld joints.

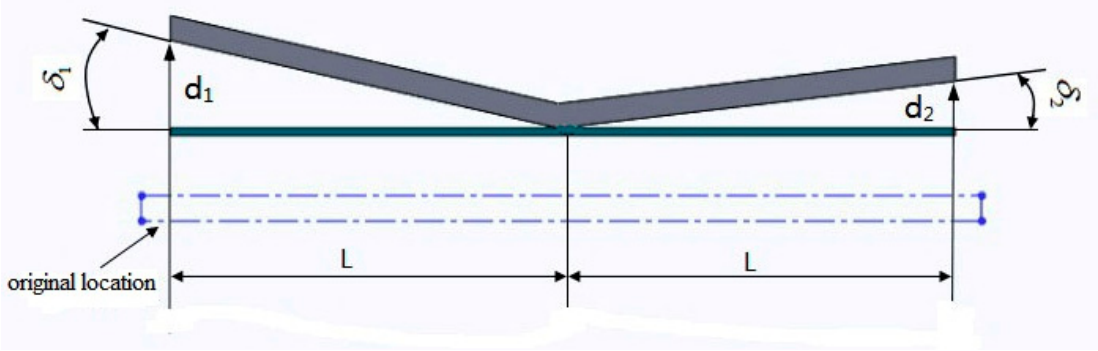

Figure 14. Angular distortion calculation model.

It is known that the width (L) of the Q690D high-strength steel welded test plate is 120 mm. According to Figure 14 and Equation (1), the deformation angle of the welding plate of the LTT joint and ER110S-G joint can be calculated respectively:

$$\delta_{LTT} = \delta_1 + \delta_2 = \frac{d_1 + d_2}{L} = \frac{4.5}{120} = 0.0375 \tag{2}$$

$$\delta_{ER110S-G} = \delta_1 + \delta_2 = \frac{d_1 + d_2}{L} = \frac{7.5}{120} = 0.0625 \tag{3}$$

According to the above results, the use of low transformation temperature (LTT) wire as the weld filler metal resulted in a welding test plate angle deformation of 0.0375 rad, while the use of common ER110S-G wire as the weld filler metal resulted in a welding test plate angle deformation of 0.0625 rad. Thus, it can be concluded that the amount of angular deformation of the LTT joint is only 60% of the ER110S-G joint.

4. Conclusions

One kind of low transformation temperature (LTT) wire for reducing welding residual stress of Q690D low-alloy high-strength steel has been developed. Using Q690D steel for the base plates, two weld fillers, namely self-developed LTT wire and ordinary ER110S-G, were studied. The effect of different filling materials on microstructure, mechanical properties, phase-transition temperature, and welding residual stress and deformation was compared and analyzed, and the following conclusions were drawn:

(1) The microstructure of the LTT joint is mainly composed of martensite and residual austenite, while the microstructure of the ER110S-G joint is mainly composed of a large number of acicular ferrite and a small amount of granular bainite.

(2) The peak microhardness of the weld zone of the LTT joint was 383 HV, significantly higher than that of the base metal (265~275 HV). The microhardness of the weld zone of the ER110S-G joint was 255 HV.

(3) The impact absorbing energy of the weld zone of the ER110S-G joint is 105 J, while the impact absorbing energy of the weld zone of the LTT joint is only 36 J, far below that of the ER110S-G weld impact absorbing energy.

(4) The LTT joint has tensile strength of 793~801 MPa, with elongation of 9.8%, while the ER110S-G joint has tensile strength of 781~794 MPa and elongation of 13.6%.

(5) The martensitic phase transformation of LTT starts at 212 °C and finishes at around 50 °C, and the expansion caused by phase transition is about 0.48%, which is much higher than that of the base metal (0.15%) and ER110S-G (0.18%).

(6) The residual tensile stress at the weld zone of the ER110S-G joint is 175.5 MPa, while the residual compressive stress at the weld zone of the LTT joint is −257.6 MPa. These results show that the low transformation temperature (LTT) wire can produce compressive stress, which is helpful in improving the joint performance.

(7) After welding, the distortion radian of LTT and ER110S-G joints are 0.0375 rad and 0.0625 rad, respectively. The distortion radian of LTT joint is only 60% of ER110S-G joint, with the main reason for this result being the residual stress state change.

Author Contributions: Conceptualization, X.C.; Methodology, X.C.; Software, P.W., Q.P., S.L.; Experimental work, P.W.; Validation, X.C., P.W., Q.P., S.L.; Formal Analysis, X.C.; Investigation, X.C., P.W., Resources, X.C., Q.P., S.L.; Data Curation, X.C., P.W., Q.P.; Writing-Original Draft Preparation, X.C., P.W.; Writing-Review & Editing, X.C.; Visualization, X.C., S.L.; Supervision, X.C., Q.P.; Project Administration, X.C., S.L.

Funding: This research was funded by the National Natural Science Foundation of China under Grant No. 51575401 and Zhejiang Provincial Natural Science Foundation under Grant No. LY16E050007, this work is also partly sponsored by State Key Lab of Advanced Welding and Joining, Harbin Institute of Technology No. AWJ-16-M01.

Acknowledgments: This work is sponsored by the National Natural Science Foundation of China under Grant No. 51575401 and Zhejiang Provincial Natural Science Foundation under Grant No. LY16E050007, this work is also partly sponsored by State Key Lab of Advanced Welding and Joining, Harbin Institute of Technology (No. AWJ-16-M01).

Conflicts of Interest: The authors declare no conflicts of interest.

References

1. Liu, Y.; Shi, L.; Liu, C.; Yu, L.; Yan, Z.; Li, H. Effect of step quenching on microstructures and mechanical propertiesof HSLA steel. *Mater. Sci. Eng. A* **2016**, *675*, 371–378. [CrossRef]
2. Ramesh, R.; Dinaharan, I.; Kumar, R.; Akinlabi, E.T. Microstructure and mechanical characterization of friction stir welded highstrength low alloy steels. *Mater. Sci. Eng. A* **2017**, *687*, 39–46. [CrossRef]
3. Kouadri-Henni, A.; Seang, C.; Malard, B.; Klosek, V. Residual stresses induced by laser welding process in the case of adual-phase steel DP600: Simulation and experimental approaches. *Mater. Des.* **2017**, *123*, 89–102. [CrossRef]

4. Alipooramirabad, H.; Paradowska, A.; Ghomashchi, R.; Reid, M. Investigating the effects of welding process on residual stresses, microstructure and mechanical properties in HSLA steel welds. *J. Manuf. Process.* **2017**, *28*, 70–81. [CrossRef]
5. Ferro, P.; Berto, F.; James, N.M. Asymptotic residual stress distribution induced by multipass welding processes. *Int. J. Fatigue* **2017**, *101*, 421–429. [CrossRef]
6. Kartal, M.E.; Kang, Y.H.; Korsunsky, A.M.; Cocks, A.C.; Bouchard, J.P. The influence of welding procedure and plate geometry on residual stresses in thick components. *Int. J. Solids Struct.* **2016**, *80*, 420–429. [CrossRef]
7. Ramjaun, T.; Stone, H.J.; Karlsson, L.; Kelleher, J.; Moat, R.J.; Kornmeier, J.R.; Dalaei, K.; Bhadeshia, H.K. Effect of interpass temperature on residual stresses in multipass welds produced using low transformation temperature filler alloy. *Sci. Technol. Weld. Join.* **2014**, *19*, 44–51. [CrossRef]
8. Harati, E.; Karlsson, L.; Svensson, L.E.; Dalaei, K. Applicability of low transformation temperature welding consumables to increase fatigue strength of welded high strength steels. *Int. J. Fatigue* **2017**, *97*, 39–47. [CrossRef]
9. Kang, H.T.; Lee, Y.L.; Sun, X.J. Effects of residual stress and heat treatment on fatigue strength of weldments. *Mater. Sci. Eng. A* **2008**, *497*, 37–43. [CrossRef]
10. Dai, H.; Francis, J.A.; Stone, H.J.; Bhadeshia, H.K.; Withers, P.J. Characterizing phase transformations and their effects on ferritic weld residual stresses with X-rays and neutrons. *Metall. Mater. Trans. A* **2008**, *39*, 3070–3078. [CrossRef]
11. Shiga, C.; Murakawa, E.; Matsuo, Y.; Ohsuga, U.; Hiraoka, K.; Morikage, Y.; Yasuda, K. Fatigue improvement in high-strength steel welded joints with compressive residual stress. *Weld. World* **2014**, *58*, 55–64. [CrossRef]
12. Ohta, A. Fatigue strength improvement by using newly developed low transformation temperature welding material. *Weld. World* **1999**, *43*, 38–42.
13. Barsoum, Z.; Gustafsson, M. Fatigue of high strength steel joints welded with low temperature transformation consumables. *Eng. Fail. Anal.* **2009**, *16*, 2186–2194. [CrossRef]
14. Scandella, F.; Cavallin, N.; Gressel, P.; Haouas, J.; Jubin, L.; Lefebvre, F.; Huther, I. Use of martensitic stainless steel welding consumable to substantially improve the fatigue strength of low alloy steel welded structures. *Procedia Eng.* **2013**, *66*, 108–125. [CrossRef]
15. Wang, W.; Huo, L.; Zhang, Y.; Wang, D.; Jing, H. New developed welding electrode for improving the fatigue strength of welded joints. *J. Mater. Sci. Technol.* **2002**, *18*, 527–531.
16. Altenkirch, J.; Gibmeier, J.; Kromm, A.; Kannengiesser, T.; Nitschke-Pagel, T.; Hofmann, M. In situ study of structural integrity of low transformation temperature (LTT)-welds. *Mater. Sci. Eng. A* **2011**, *528*, 5566–5575. [CrossRef]
17. Miki, C.; Hanji, M.T.; Tokunaga, M.K. Weld repair for fatigue-cracked joints in steel bridges by applying low temperature transformation welding wire. *Weld. World* **2013**, *56*, 40–50. [CrossRef]
18. Zenitani, S.; Hayakawa, N.; Yamamoto, J.; Hiraoka, K.; Morikage, Y.; Kubo, T.; Yasuda, K.; Amano, K. Development of new low transformation temperature welding consumable to prevent cold cracking in high strength steel welds. *Q. J. Jpn. Weld. Soc.* **2005**, *23*, 95–102. [CrossRef]
19. Mikami, Y.; Mochizuki, M.; Toyoda, M.; Morikage, Y. Measurement and numerical simulation of angular distortion of fillet welded T-joints—Welding angular distortion control by transformation expansion of weld metals. *Weld. Int.* **2007**, *21*, 547–560. [CrossRef]
20. Mikami, Y.; Morikage, Y.; Mochizuki, M.; Toyoda, M. Angular distortion of fillet welded T joint using low transformation temperature welding wire. *Sci. Technol. Weld. Join.* **2009**, *14*, 97–105. [CrossRef]
21. Mikami, Y.; Mochizuki, M.; Toyoda, M. Effect of characteristics of transformation expansion of weld metals on angular distortion behavior of welded joints. *Q. J. Jpn. Weld. Soc.* **2007**, *25*, 59–67. [CrossRef]
22. Kromm, A.; Dixneit, J.; Kannengiesser, T. Residual stress engineering by low transformation temperature alloys-state of the art and recent developments. *Weld. World* **2014**, *58*, 729–741. [CrossRef]
23. Shirzadi, A.A.; Bhadeshia, H.K.; Karlsson, L.; Withers, P.J. Stainless steel weld metal designed to mitigate residual stresses. *Joining* **2009**, *14*, 559–565. [CrossRef]